The Effect and Influence of *cis*-Ligands on the Electronic and Oxidizing Properties of Nonheme Oxoiron Biomimetics. A Density Functional Study†

Sam P. de Visser*,‡ and Wonwoo Nam*,§

The Manchester Interdisciplinary Biocenter and the School of Chemical Engineering and Analytical Science, The University of Manchester, 131 Princess Street, Manchester, M1 7DN, U.K., and Department of Chemistry, Division of Nano Sciences, and Centre for Biomimetic Systems, Ewha Womans University, Seoul 120-750, Korea

Received: March 3, 2008; Revised Manuscript Received: May 12, 2008

Density functional theory studies on the nature of the cis effect and cis influence of ligands on oxoiron nonheme complexes have been performed. A detailed analysis of the electronic and oxidizing properties of $[Fe^{IV}{=}O(TPA)L]^+$ with L = F^-, Cl^-, and Br^- and TPA = tris-(2-pyridylmethyl)amine are presented and compared with $[Fe^{IV}{=}O(TPA)NCCH_3]^{2+}$. The calculations show that the electronic cis effect is determined by favorable orbital overlap between first-row elements with the metal, which are missing between the metal and second- and third-row elements. As a consequence, the metal 3d block is split into a one-below-two set of orbitals with L = Cl^- and Br^-, and the HOMO/LUMO energy gap is widened with respect to the system with L = F^-. However, this larger HOMO/LUMO gap does not lead to large differences in electron affinities of the complexes. Moreover, a quantum mechanical analysis of the binding of the ligand shows that it is built up from a large electric field effect of the ligand on the oxoiron species and a much smaller quantum mechanical effect due to orbital overlap. These contributions are of similar strength for the three tested halogen cis ligands and result in similar reactivity patterns with substrates. The calculations show that $[Fe^{IV}{=}O(TPA)L]^+$ with L = F^-, Cl^-, and Br^- have closely lying triplet and quintet spin states, but only the quintet spin state is reactive with substrates. Therefore, the efficiency of the oxidant will be determined by the triplet−quintet spin state crossing of the reaction. The reaction of styrene with a doubly charged reactant, that is, $[Fe^{V}{=}O(TPA)L]^{2+}$ with L = F^-, Cl^-, and Br^- or $[Fe^{V}{=}O(TPA)NCCH_3]^{3+}$, leads to an initial electron transfer from the substrate to the metal followed by a highly exothermic epoxidation mechanism. These reactivity differences are mainly determined by the overall charge of the system rather than the nature of the cis ligand.

Introduction

Heme enzymes appear in nature in many varieties and are involved in oxygen transport as well as monooxygenase properties.[1] The active-site heme is linked to the protein backbone through one of the iron ligands called the axial ligand. This axial ligand is a histidine side chain in peroxidases, a tyrosinate in catalases, and often a cysteinate in the cytochromes P450.[2] These enzymes all have different functions in biosystems: peroxidases detoxify hydrogen peroxide to water, whereas the cytochromes P450 catalyze monooxygenation reactions.[1] These heme enzymes have a central iron atom that is linked to the protein backbone via its axial ligand. Trans to this axial ligand (on the distal side of the heme) binds either molecular oxygen or hydrogen peroxide. In monooxygenases, the iron−dioxygen complex is converted into an oxoiron active species via a series of proton- and electron-transfer steps. It is the nature of this axial ligand that has been implicated in the functional differences of the heme-containing enzymes.[3] In particular, cysteinate elicits a push effect and makes the iron more electron-rich, whereas histidine withdraws electrons from iron.[3]

In order to quantify the effect of the axial ligand of heme systems, many systematic studies have been performed on synthetic biomimetic models.[4–8] Thus, a series of oxoiron(IV) tetramesitylporphyrin $[Fe^{IV}{=}O(TMP^{+\bullet})L]$ oxidants with variable axial ligand L = F^-, CH_3OH, Cl^-, acetate, $CF_3SO_3^-$, and ClO_4^- were prepared.[4] Oxidation of styrene by these systems identified a strong axial ligand effect with the system with L = F^- that resulted in the highest reactivity, whereas the one with L = ClO_4^- was the least reactive oxidant under the same experimental conditions. Thus, it appears that the axial ligand elicits a trans effect on the oxoiron catalytic center that results in differences in reactivity patterns with substrates. In addition, also a trans influence was identified that created spectroscopic changes as a consequence of the axial ligand.[5] An example of the trans influence is the frequency for the Fe−O stretch vibration ($\upsilon_{Fe=O}$) that shifts in value on the basis of the push/pull effect of the axial ligand. The trans effect results in different reactivity patterns with substrates and was assigned to the fact that some systems can stabilize intermediates with the metal in oxidation state Fe^{III}, whereas others keep the metal in the Fe^{IV} oxidation state.[6] For the series L = NO_3^-, $CF_3SO_3^-$, ClO_4^-, acetate, Cl^-, and OH^-, the oxidizing efficiency was found to decrease.[7] Density functional studies on the axial ligand effect showed that the reaction barriers correlate with the electron affinity (EA) of the oxidant.[8]

Many studies on biomimetic complexes have established regioselective product formation with product distributions varying for systems with different axial ligands. For instance, Groves et al., showed that the reaction of $Fe^{IV}{=}O(TMP^{+\bullet})Cl$

† Part of the "Sason S. Shaik Festschrift".

* Corresponding authors. E-mail: sam.devisser@manchester.ac.uk and wwnam@ewha.ac.kr.

‡ The University of Manchester.

§ Ewha Womans University.

10.1021/jp8018556 CCC: $40.75
Published on Web 07/11/2008

with cyclohexene gives either cyclohexene oxide or cyclohexen-3-ol products in a ratio of 14:1.[9] The product ratios, however, were found to be dependent on the nature of the reaction conditions as well as of the axial ligand. Further studies with electron-rich porphyrin ligands gave predominantly cyclohexen-3-ol products at low temperatures but epoxides at higher temperatures.[10] However, with an electron-deficient porphyrin ligand, no regioselectivity reversal was obtained, and only epoxide products were detected. These studies are in agreement with theoretical studies on the regioselectivity of propene epoxidation versus hydroxylation by a P450 CpdI model.[11] Thus, the gas-phase calculations give dominant epoxide products, but the inclusion of hydrogen bonding toward the thiolate group that mimics the hydrogen-bonding interactions in the enzyme changes the regioselectivity in favor of hydroxylation. Experimental studies on the temperature dependence on regioselective hydroxylation versus epoxidation showed that hydroxylation reactions are entropically controlled, whereas epoxidation mechanisms are enthalpically controlled, which was confirmed with theoretical calculations.[12]

Recently, it was shown that also the axial ligand (L) of nonheme oxoiron systems influences the electronic properties of the oxidant and its reactivity patterns.[13] Thus, combined experimental and density functional theory (DFT) studies on the oxo-transfer reaction of Fe^{IV}═O(TMC)L with TMC = 1,4,8,11-tetramethyl-1,4,8,11-tetraazacyclotetradecane to substrates were investigated. In particular, two different reactions were studied, namely, the oxygenation of PPh_3 and the hydroxylation of aromatic substrates. It was shown that the oxo-transfer reaction is proportional to the electrophilicity of the oxoiron group, which is influenced by the push effect of electrons of the axial ligand. By contrast, the hydrogen-atom abstraction reactions were found to correlate with the reduction potential of the oxoiron oxidant. The reactivity patterns were also shown to be dependent on the triplet−quintet energy gap of the reactant, especially because nonheme and heme-type oxoiron species react via two-state reactivity patterns (TSR) on closely lying spin states.[14]

Despite many efforts to quantify the axial (trans) ligand effect and the trans influence of ligands on the oxoiron system, only a few studies have been devoted to the effect of ligands perpendicular to the oxoiron group, that is, cis ligands. In fact, only one recent study establishes a cis effect on the oxoiron group and that it is different from a trans effect.[15] It was anticipated that electronic effects presumably are the consequence of the difference between a cis and a trans effect. To find out whether ligands perpendicular to the oxoiron group can influence the electronic properties of the oxidant and its reactivity patterns, we have studied a nonheme oxoiron system with variable cis ligands. Our studies used a tripodal tetradendate ligand: TPA = tris-(2-pyridylmethyl)amine, see Scheme 1. The oxoiron(TPA) system, therefore, has an available ligand site perpendicular to the oxoiron bond that is usually occupied by a solvent molecule or an anionic ligand. In this work, we report DFT studies on the electronic properties of $[Fe{=}O(TPA)L]^+$ with L = F^-, Cl^-, and Br^- and $[Fe{=}O(TPA)NCCH_3]^{2+}$ and their reactivity patterns with respect to styrene.

Recently, experimental studies on $[Fe^{IV}{=}O(TPA)L]^+$ with L = CF_3COO^-, Cl^-, and Br^- reported Mössbauer parameters and EXAFS structural data.[16] These studies suggested this system to be useful for cis-effect studies on the effect of the oxoiron system. A recent DFT investigation of $[Fe^{IV}{=}O(TPA)Cl]^+$ and $[Fe^{V}{=}O(TPA)Cl]^{2+}$ with cyclohexane focused on the regioselective chlorination versus hydroxylation reactions.[17] The results showed that the Fe^V complex can regioselectively chlorinate the substrate without hydroxylation products, whereas the Fe^{IV} complex gives a mixture of reaction products. Thus, as hydroxylation reactions give halogenation byproduct, we report here studies of the epoxidation of styrene because that reaction is not expected to give side reactions leading to, for example, halogenations.

SCHEME 1: Schematic Representation of an Isolated TPA Group and as Part of an Oxoiron Complex $[Fe{=}O(TPA)L]^+$ with L Being the Variable cis Ligand in Our Studies[a]

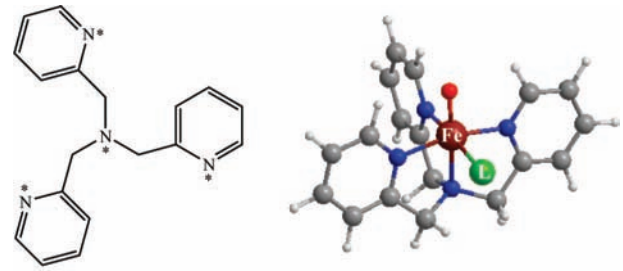

TPA ligand $[Fe{=}O(TPA)L]^+$

[a] The atoms labeled with a star bind to iron.

Methods

Our procedures are similar to previous calculations in the field, which we will briefly summarize here.[18,19] We calculated the lowest lying electronic states of $[Fe^{IV}O(TPA)L]^+$ with L = F^-, Cl^-, and Br^- as well as $[Fe^{IV}O(TPA)NCCH_3]^{2+}$ and their one-electron reduced and oxidized forms. These systems have closely lying spin states and tend to react with TSR;[14] therefore, we tested each system in the singlet, triplet, and quintet spin states. The one-electron reduced and oxidized forms were calculated in the lowest lying doublet, quartet, and sextet spin states. The overall spin state of the structure is identified with a superscript next to the label. To test whether cis substitution of the oxidant influences reactivity patterns, we calculated the epoxidation of styrene by $[Fe^{IV}O(TPA)L]^{+/2+}$ and $[Fe^{V}O(TPA)L]^{2+/3+}$ with L = F^-, Cl^-, Br^-, and $NCCH_3$.

All structures were fully optimized without constraints in the Jaguar 7.0 program package, followed by an analytical frequency calculation in Gaussian-03.[20,21] The local minima described here had real frequencies only, and the transition states are characterized by a single imaginary frequency for the correct mode. We used the unrestricted hybrid density functional method UB3LYP in combination with a double-ζ quality LACVP basis set on Fe and Br and 6-31G on the rest of the atoms (basis set B1).[22,23] Subsequent single-point calculations with a triple-ζ quality LACV3P+ basis set on Fe and Br and 6-311+G* on the rest of the atoms was done to correct the energies (basis set B2). All energies reported in this work are obtained with UB3LYP/B2 with ZPE corrections at UB3LYP/B1. Free energies (G) were calculated from the absolute energies (obtained with basis set B2) corrected for ZPE and with thermal and entropic corrections with basis set B1. Vibrational frequencies reported were scaled with a factor of 0.9614 as recommended by Scott and Radom.[24]

To test the effect of the environment on the spin splitting, we ran single-point calculations in Jaguar with a dielectric constant of $\varepsilon = 5.7$ and a probe radius of 2.7.

The oxidizing properties of the $[Fe^{IV}O(TPA)L]^{+/2+}$ with L = F^-, Cl^-, Br^-, and $NCCH_3$ toward styrene were calculated on the lowest lying triplet and quintet spin state surfaces for the Fe^{IV} systems and on the quartet spin state surface for the

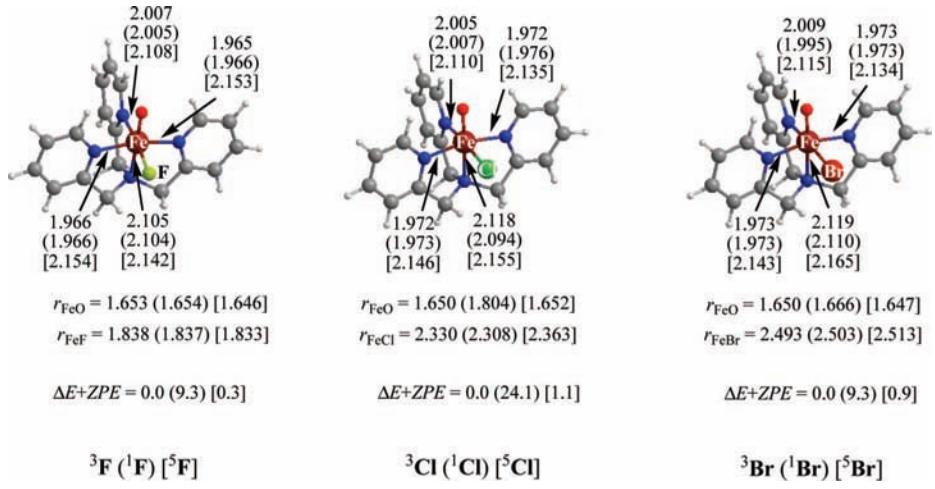

Figure 1. Optimized geometries of Fe=O(TPA)F$^+$ (**F**), Fe=O(TPA)Cl$^+$ (**Cl**), and Fe=O(TPA)Br$^+$ (**Br**) in the triplet, singlet, and quintet spin states. All bond lengths are in Ångstroms, and relative energies (with respect to the triplet state) are in kcal mol^{-1}.

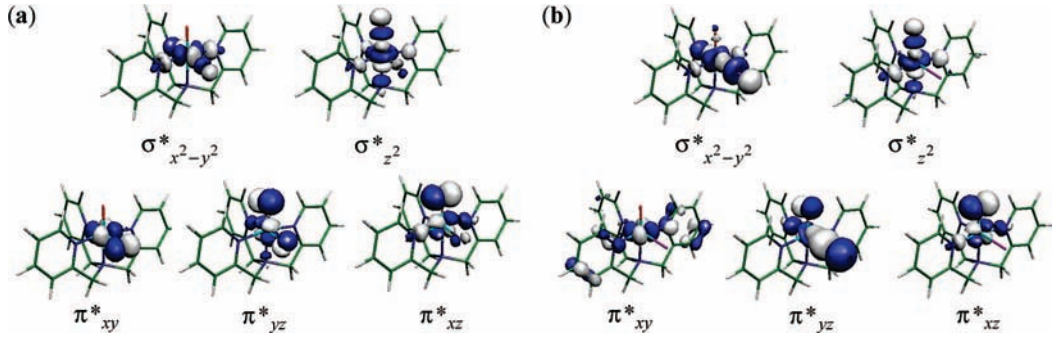

Figure 2. High-lying occupied and low-lying virtual orbitals of ^{3}[Fe=O(TPA)F]$^+$ (a) and ^{3}[Fe=O(TPA)Br]$^+$ (b).

Fe^V species. Initially, detailed geometry scans (with one degree of freedom fixed) were performed to explore the shape of the potential energy surface, see Supporting Information. The maxima of these scans were used as starting points of the transition-state geometry optimizations.

Results and Discussion

TPA binds to iron as a tetradentate ligand in a tripodal fashion, see Scheme 1. The fifth ligand usually binds a solvent molecule or anionic ligand such as a halide anion, whereas the sixth ligand is the place where the oxo group binds. Varying the fifth ligand in this system, therefore, should give an estimate of the cis effect and cis influence of ligands on the metal and oxoiron groups and the oxidizing power of the system. Thus, our initial studies on these systems are focused on the geometric differences, HOMO/LUMO gaps, orbital ordering, and EA differences of the oxidants. In a second series of calculations, we studied the oxidizing differences with respect to styrene epoxidation of a series of [Fe^{IV}=O(TPA)L]$^{+/2+}$ systems with variable cis ligand, L = F$^-$, Cl$^-$, Br$^-$, and NCCH$_3$. In the first part of the paper, however, we will focus on the systems with the same metal oxidation state and overall charge only which are substituted with a halide anion.

Geometric Differences of [Fe^{IV}=O(TPA)L]$^+$ Oxidants. Figure 1 shows the optimized geometries of [Fe^{IV}=O(TPA)L]$^+$ with L = F$^-$, Cl$^-$, and Br$^-$ in the lowest lying singlet, triplet, and quintet spin states. For simplicity, we abbreviate these systems by the cis ligand written in bold; that is, **F** represents Fe=O(TPA)F$^+$, **Cl** is Fe=O(TPA)Cl$^+$, and **Br** stands for Fe=O(TPA)Br$^+$. The spin multiplicity is given in superscript next to this symbol.

Generally, oxoiron systems have a series of high-lying occupied and low-lying virtual orbitals that are close in energy.[25] As a result, these systems can exist in several possible spin states, and the ordering of those is dependent on the other ligands bound to iron as well as environmental perturbations.[26] In the triplet spin state, all systems have occupation $\pi^*_{xy}{}^2\ \pi^*_{xz}{}^1\ \pi^*_{yz}{}^1$, whereas the lowest lying quintet spin state has occupation $\pi^*_{xy}{}^1\ \pi^*_{xz}{}^1\ \pi^*_{yz}{}^1\ \sigma^*_{x^2-y^2}{}^1$ (see below). In the gas phase, the triplet spin state is the ground state for **F**, **Cl**, and **Br**, but the quintet spin states are only 0.3−1.1 kcal mol^{-1} higher in energy. Therefore, similarly to other heme and nonheme oxoiron complexes, it is expected that **F**, **Cl**, and **Br** will react via TSR on competing triplet and quintet spin state surfaces.[14] Interestingly, there does not seem to be an effect of the cis ligand on the spin state ordering and relative energies for the systems shown in Figure 1. The singlet spin state in all cases is a high-lying spin state and will not play an important role. Therefore, the singlet spin states of these systems were not further taken into consideration in the remainder of this study. Because of differences in orbital occupation in ^{1}**Cl** with respect to ^{1}**F** and ^{1}**Br**, the chloride system is elevated in energy relative to its triplet and quintet spin state structures.

The oxoiron bond is in the range of 1.646−1.666 Å, typical for a double bond. This value is in good agreement with experimental and theoretical studies of oxoiron bonds obtained for heme and nonheme systems.[27,28] Thus, Krebs et al. determined an Fe−O distance of 1.62 Å for the active species of taurine/α-ketoglutarate dioxygenase enzyme, whereas Que et al. determined a value of 1.646 Å for a nonheme biomimetic complex.[27a,b] The Fe−N bonds show little variation except that they are longer in the quintet spin state. This is as expected

because the $\sigma^*_{x^2-y^2}$ orbital is singly occupied in the quintet spin state which results in elongation of the Fe−N bonds (vide infra). Minor variations are observed in the iron−halogen bond distances between the different spin states. It appears therefore that the spin state has minor effect on the Fe−L distances.

From the frequency calculations of ^{3}**F**, ^{3}**Cl**, and ^{3}**Br**, we extracted the characteristic stretch vibrations of the metal with the oxo, axial, and cis ligands. Thus, the Fe−O stretch vibration is found at 814.5, 834.7, and 834.9 cm^{-1} for ^{3}**F**, ^{3}**Cl**, and ^{3}**Br**, respectively. Therefore, the fluoride cis ligand creates a cis influence and a lowering of the Fe−O stretch vibration by about 20 cm^{-1}, whereas the chloride- and bromide-substituted systems appear identical. Interestingly, the cis influence of the fluoride anion is only found on the Fe−O stretch vibration because the Fe−N_{axial} stretch vibration stays virtually constant at 864.4 ± 1 cm^{-1} for the three systems. Obviously, the vibrational frequency for the Fe−L stretching mode is dependent on the size and mass of atom L and is largest for fluoride (555.3 cm^{-1}), somewhat smaller for chloride (374.8 cm^{-1}), and the smallest for bromide (356.1 cm^{-1}).

The calculated oxoiron stretch vibrations of ^{3}**F**, ^{3}**Cl**, and ^{3}**Br** are in the range of values obtained for oxoiron porphyrin systems with variable axial ligands.[5,29] It has been shown that the modified Badger rule can predict the values of Fe=O frequencies via

$$r_e = 0.74 + 1.54(K)^{-1/3} \quad (1)$$

In this equation, r_e represents the equilibrium bond length of the Fe−O bond, and K is the force constant of the vibrational mode.[30] By using the Fe−O distances of ^{3}**F**, ^{3}**Cl**, and ^{3}**Br** from Figure 1, force constants of 4.80 mdyn/Å for ^{3}**F** and 4.85 mdyn/Å for ^{3}**Cl** and ^{3}**Br** are obtained. These force constants imply identical vibrational frequencies for ^{3}**Cl** and ^{3}**Br** as indeed observed from our frequency calculations. The slightly smaller force constant for ^{3}**F** results in an increase of the vibrational frequency, as indeed observed in the calculations.

Electronic Differences Due to Cis Substitution. Although geometrically, the three oxidants (**F**, **Cl**, and **Br**) give virtually the same optimized structures (see Figure 1), there are subtle electronic differences due to ligand binding to the metal. Figure 2 shows the high-lying occupied and low-lying virtual orbitals of ^{3}[Fe=O(TPA)F]$^+$ and ^{3}[Fe=O(TPA)Br]$^+$. The orbitals of ^{3}[Fe=O(TPA)Cl]$^+$ resemble those obtained with the bromide ligand closely and have been omitted. The two sets of orbitals in Figure 2 are dominated by contributions from the 3d atomic orbitals on iron and have been labeled as such (3d label in subscript). The metal 3d orbitals split into a typical $t_{2g}-e_g$ set of orbitals with three low-lying π^* orbitals and two virtual σ^* orbitals. The z-axis has been taken along the Fe−O bond, whereas the y-axis is along the Fe−L bond. With fluoride as cis ligand, the lowest-lying orbital is the π^*_{xy} orbital representing the antibonding interactions of the $3d_{xy}$ atomic orbital on iron with the $2p_x$ orbital on fluoride. The π^*_{xz} and π^*_{yz} orbitals are formed through antibonding interactions of the $3d_{xz}/3d_{yz}$ atomic orbitals on iron with the $2p_x/2p_y$ atomic orbitals on oxygen. The π^*_{xz} orbital also has small contributions on the nitrogen atoms along the x-axis, whereas the π^*_{yz} orbital interacts with the fluoride as well as with the nitrogen atom opposite of it. The $\sigma^*_{x^2-y^2}$ orbital is described by interactions of the metal with the three nitrogen atoms and the fluoride atom in the xy-plane of symmetry, whereas the $\sigma^*_{z^2}$ orbital is antibonding between the metal and the oxo and axial nitrogen atom.

Because a chloride and a bromide atom are larger in size than a fluoride atom, the Fe−L distance is much larger as well. As a result, different atomic orbitals interact between iron and its cis ligand chloride/bromide. Thus, the orbital overlap between $3d_{xy}$ on iron with $3p_x/4p_x$ on the halide similarly to π^*_{xy}(**F**) in Figure 2a is energetically unfavorable because of the large interatomic distance of the two atoms. Instead, the π^*_{xy} orbital in **Cl** and **Br** interacts with 2p orbitals on the nitrogen atoms along the x-axis.

The π^*_{yz} orbital for ^{3}[Fe=O(TPA)Cl]$^+$ and ^{3}[Fe=O(TPA)Br]$^+$ interacts now with the $3p_y/4p_y$ atomic orbital on the halogen atom, which is more diffuse than the $2p_y$ orbital on fluoride. The π^*_{xz} and $\sigma^*_{z^2}$ orbitals are similar in shape and size for all the halogen containing systems. The $\sigma^*_{x^2-y^2}$ has a strong contribution from the halogen atom for L = Cl^- and Br^-. As a consequence of the differences in orbital levels and HOMO−LUMO energy gaps for the ^{3}[Fe=O(TPA)L]$^+$ with L = F^-, Cl^-, and Br^- series of oxidants, also differences in electron affinities, spin-state ordering, and maybe even oxidizing properties of the three systems are expected.

As follows from the molecular orbitals shown in Figure 2, there are distinct differences between ^{3}**F** on the one hand and ^{3}**Cl**/^{3}**Br** on the other hand. To show the effects of the orbital shapes on the relative energies of the orbitals, we display the orbital energy levels of ^{3}**F**, ^{3}**Cl**, and ^{3}**Br** in Figure 3. In ^{3}**F**, all π^* orbitals are within 0.35 eV of each other, as expected from the large similarities in the molecular orbitals (see Figure 2). In ^{3}**Cl** and ^{3}**Br**, by contrast, the π^*_{xy} orbital is significantly lower in energy, and the three π^* orbitals split into a one-below-two set of orbitals. The energy difference between π^*_{xz} and π^*_{yz} remains more or less the same in all systems. Similarly, the $\sigma^*_{x^2-y^2}$ orbital is stabilized with respect to the $\sigma^*_{z^2}$ orbital much more strongly in ^{3}**Cl** and ^{3}**Br** than in ^{3}**F**. Therefore, the cis effect on the electronic properties of the oxidants manifests itself through favorable orbital interactions. These interactions are beneficial for first-row elements and weaker for second- and third-row elements.

The HOMO/LUMO energy gap for **F** is 4.28 eV, whereas it is 4.87 eV (**Cl**) and 4.82 eV (**Br**) for the systems with heavier halides. Because a reaction of the oxoiron species results in a two-electron reduction of the iron(TPA)L system, this HOMO/LUMO gap should give us a suggestion of which of these systems is most likely to be a better oxidant. In this particular case, the HOMO/LUMO gap implicates ^{3}**F** as likely to be a much better oxidant than ^{3}**Cl** and ^{3}**Br**.

Recent studies of the axial ligand effect showed that the $\pi^*_{xy}/\sigma^*_{x^2-y^2}$ energy difference is proportional to the triplet−quintet energy gap.[13b] As follows from Figure 3, the $\pi^*_{xy}/\sigma^*_{x^2-y^2}$ energy gap is 5.64, 5.79, and 5.63 eV, for ^{3}**F**, ^{3}**Cl**, and ^{3}**Br**, respectively. Indeed, the calculated triplet−quintet energy gaps (Figure 1) of these species are very close to each other, in agreement with the calculated $\pi^*_{xy}/\sigma^*_{x^2-y^2}$ energy gap. Thus, although the π^*_{xy} orbital has more antibonding character in ^{3}**F** and therefore is higher in energy than the corresponding orbital in ^{3}**Cl** and ^{3}**Br**, this does not lead to a larger triplet−quintet energy gap because the $\sigma^*_{x^2-y^2}$ orbital in ^{3}**F** is raised with almost the same amount of energy. As can be seen from Figure 3, small effects (of less than 0.3 eV) are observed for the energy levels of the π^*_{xz}, π^*_{yz}, and $\sigma^*_{z^2}$ orbitals in ^{3}**F**, ^{3}**Cl**, and ^{3}**Br**. In conclusion, the effect of the cis ligand affects some of the high-lying occupied and low-lying virtual orbitals significantly, but not all orbitals are affected with the same amount. In particular, the π^*_{xy} and $\sigma^*_{x^2-y^2}$ are most affected, whereas only minor energetic stabilization occurs for the π^*_{xz}, π^*_{yz}, and $\sigma^*_{z^2}$ orbitals. Because the HOMO/LUMO energy gap is the difference between the

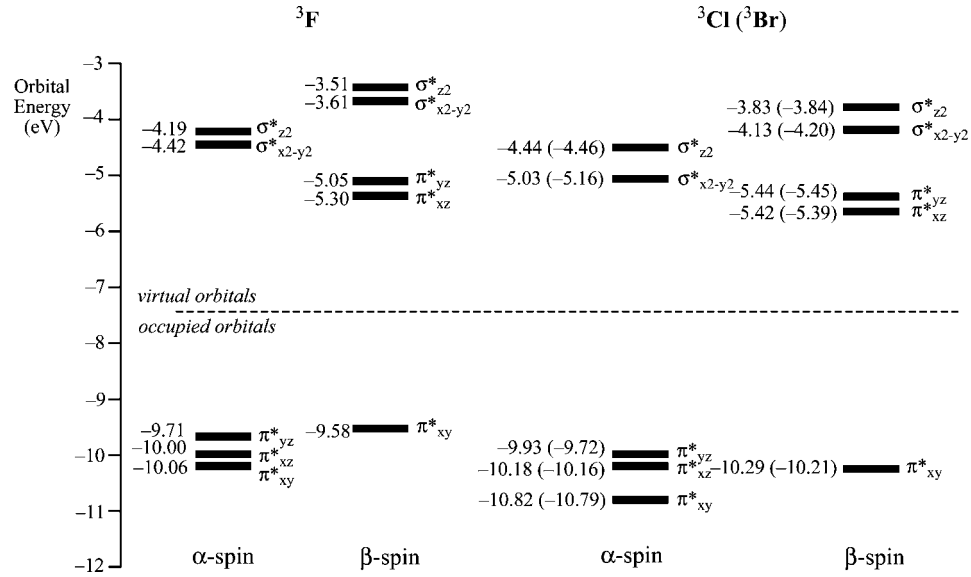

Figure 3. Orbital energy levels of ^{3}**F** (left-hand side) and ^{3}**Cl**/^{3}**Br** (right-hand side).

β-spin π^*_{xy} and π^*_{xz} orbital energies, this difference is smaller for ^{3}**F** than for ^{3}**Cl** and ^{3}**Br**.

Effect of the Cis Ligand. We estimated the effect of the cis ligand by using procedures applied to predict the axial ligand effect of the oxoiron species of P450 enzymes.[31] First, the ligand applies an electric field effect (ΔE_{Field}) on the oxoiron group because of the interaction of the charge of the ligand with the rest of the system. Second, the ligand exerts a quantum mechanical effect (ΔE_{QM}) as a result of orbital mixing after bond formation. The field and QM effects were estimated from the EA differences of the oxidant, the system where the cis ligand was replaced by a point charge and one without the cis ligand. The one-electron reduction of $[Fe{=}O(TPA)L]^+$ with L = F^-, Cl^-, and Br^- gives the EA of the oxoiron species (EA_{Oxoiron}). Subsequently, the cis ligand was removed, and single-point calculations of the oxoiron and its reduced forms were done to obtain EA_{NL}. Finally, the cis ligand was replaced by a point charge with magnitude −1, and again, the one-electron reduction potential was calculated to give EA_{PC}. Figure 4 displays these EAs as determined for the systems with the three different cis ligands.

The EA of the fluoride oxidant is 128.6 kcal mol^{-1} (5.57 eV), which is slightly smaller than the ones for chloride and bromide. The latter two are within 1 kcal mol^{-1}. Thus, ^{3}**Cl** and ^{3}**Br** have the same Fe−O stretch vibration and the same EA. To identify the individual components that contribute to the cis effect, namely, ΔE_{Field} and ΔE_{QM}, the magnitude of EA_{NL} and EA_{PC} were calculated for ^{3}**F**, ^{3}**Cl**, and ^{3}**Br**. The electric-field-effect component of the cis effect is proportional to the difference in EA between the system without cis ligand and the one where a point charge takes up the position of the ligand (eq 2).

$$\Delta E_{\text{Field}} = \text{EA}_{\text{NL}} - \text{EA}_{\text{PC}} \tag{2}$$

The QM contribution to the cis ligand, by contrast, is calculated from the EA differences of the oxoiron system and the one with a point charge in the cis position (eq 3).

$$\Delta E_{\text{QM}} = \text{EA}_{\text{PC}} - \text{EA}_{\text{Oxoiron}} \tag{3}$$

In principle, the electron affinities with a point charge in the cis position should correlate linearly with the distance of the charge from the oxoiron species. Thus, the fluoride-substituted

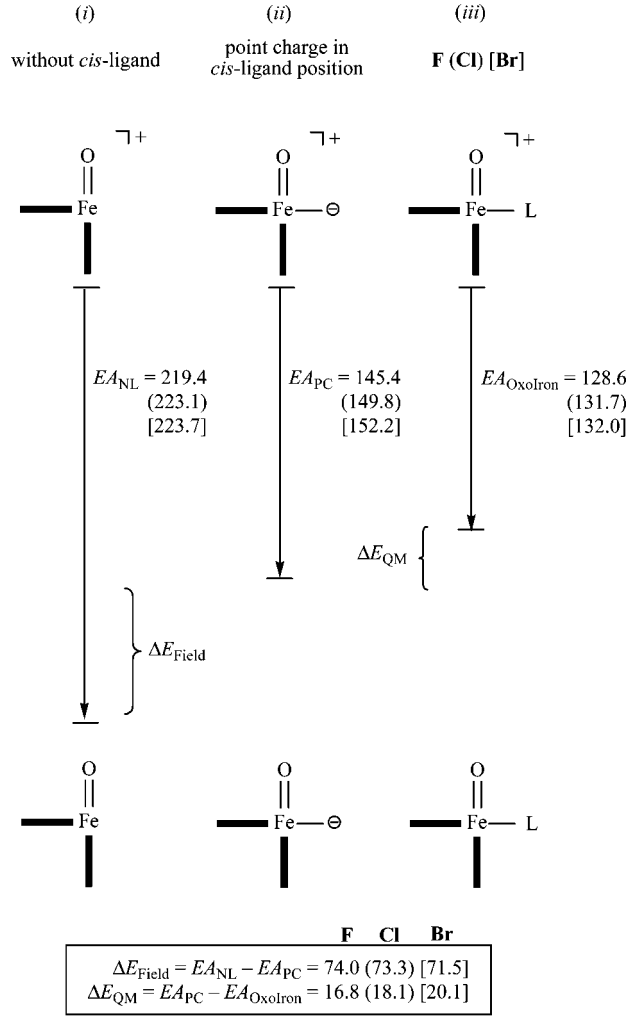

Figure 4. Effect of the cis ligand on the one electron reduction of $^3[Fe{=}O(TPA)L]^+$ with L = F^-, Cl^-, and Br^-. All energies are in kcal mol^{-1} and calculated with basis set B2. Values for EA_{Oxoiron} contain ZPE corrections to the energy.

system has the shortest Fe−L distance of 1.838 Å, whereas the distances for the chloride and bromide systems are 2.330 and 2.493 Å, respectively. Despite these large differences in atomic

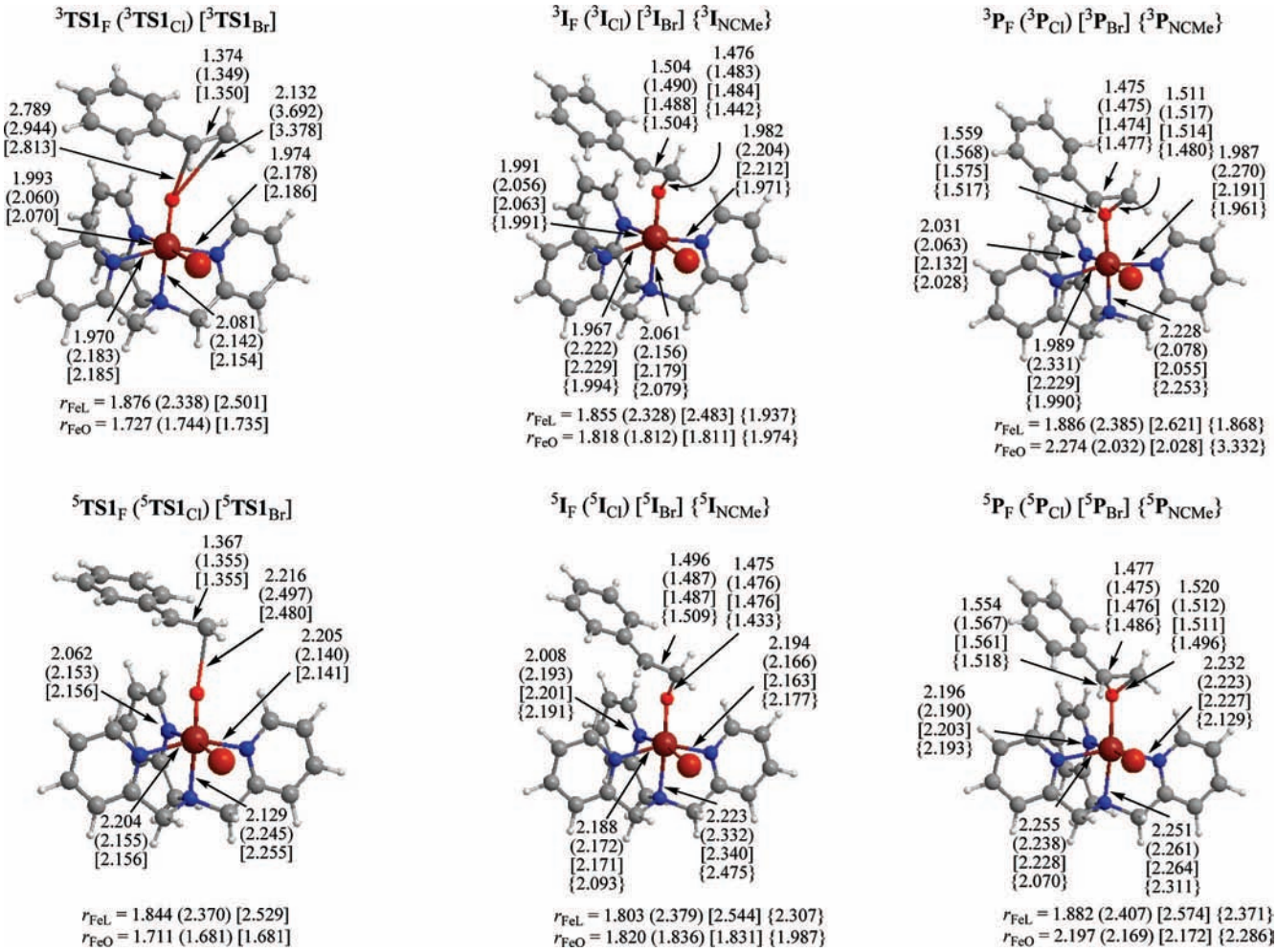

Figure 5. Optimized geometries of the rate determining transition states (^{3,5}**TS1**), radical intermediates (^{3,5}**I**), and epoxide product complexes (^{3,5}**P**) for $[Fe^{IV}{=}O(TPA)L]^{+}$ with L = F^-, Cl^-, or Br^- and $[Fe^{IV}{=}O(TPA)NCCH_3]^{2+}$. Optimized geometries in the triplet (top) and quintet (bottom) spin states are shown with bond lengths in angstroms.

distances, the value EA_{PC}(**F**) is only 4.4 kcal mol^{-1} lower in energy than EA_{PC}(**Cl**) and 6.8 kcal mol^{-1} lower than EA_{PC}(**Br**). This is due to the fact that the $\pi^*_{xy}/\sigma^*_{x^2-y^2}$ energy gap is fairly constant through the range of axial ligands chosen as discussed above.

As follows from Figure 4, the field effect of the three ligands is 74.0, 73.3, and 71.5 kcal mol^{-1} for **F**, **Cl**, and **Br**, respectively. These values are very close to the field effect obtained for a tyrosinate axial ligand in a catalase oxoiron species of 76.7 kcal mol^{-1}.[31b] By contrast, the field effect of the axial thiolate ligand in the oxoiron active species of P450 is only 54.0 kcal mol^{-1}, but this system has a strong QM effect because of the mixing of orbitals (ΔE_{QM} = 38.8 kcal mol^{-1}).[31a] The thiolate axial ligand of the active species of P450 participates in orbital mixing, for example, with a $\sigma^*_{z^2}$ orbital (similarly to the ones shown above in Figure 2) but also with several heme-type orbitals. Consequently, the oxoiron species of P450 has a singly occupied orbital with mixed heme/thiolate ligand character. Because of that, it is obvious that the QM effect of this particular axial ligand in P450 is strong. By contrast, in the catalase oxoiron system, the orbital overlap was found to be almost negligible and consequently an almost zero QM effect is obtained (ΔE_{QM} = 1.8 kcal mol^{-1}). Because of the fact that the cis ligand participates in various singly occupied molecular orbitals (see Figure 3) in $[Fe{=}O(TPA)L]^{+}$, the quantum mechanical effect of the cis ligand is non-negligible here. It is, however, not as strong as the one obtained for a thiolate axial ligand but ranging from 16.8 (**F**) to 20.1 (**Br**) kcal mol^{-1}. Therefore, the effect of changing the cis ligand from F^- to Cl^- or Br^- is small, in the order of several kcal mol^{-1} at the most. Hence, only minor differences in electronic properties, such as EAs and vibrational frequencies, are found.

Oxidizing Properties of $[Fe^{IV}{=}O(TPA)L]^{n+}$. As shown above, the cis influence gives a slightly lower Fe−O frequency for the system with F^- cis ligand in comparison to the ones with Cl^- or Br^-. In addition, the HOMO−LUMO gap of the fluoride-substituted oxidant is much smaller than those for the chloride- and bromide-substituted systems because of a raised π^*_{xy} orbital. In order to find out whether these electronic differences also create a cis effect on oxidation, we performed studies of the epoxidation of styrene by $[Fe^{IV}{=}O(TPA)L]^{+}$ with L = F^-, Cl^-, and Br^-. For comparison, we also checked the oxidizing qualities of $[Fe^{IV}{=}O(TPA)NCCH_3]^{2+}$, ^{3,5}**NCMe**. Optimized geometries are depicted in Figure 5, and the free energy landscape of the reactions is shown in Figure 6. The reactions are stepwise via a C−O bond formation transition state (**TS1**) leading to a radical intermediate (**I**) that rearranges to products (**P**) via a ring-closure transition state (**TS2**). The nature of the cis ligand is added to the label with a subscript. This mechanism is similar to the one we observed before for the alkene epoxidation by heme and nonheme oxoiron oxidants.[32] The initial C−O bond formation is the rate determining step in the reaction mechanism on all spin state surfaces.

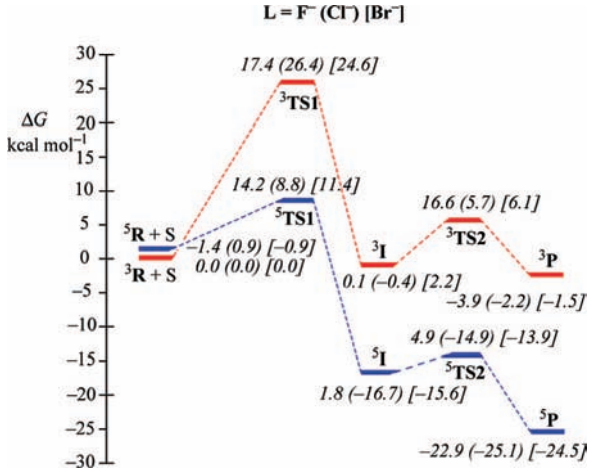

Figure 6. Free energy landscape of styrene (S) epoxidation by ^{3,5}**F**, ^{3,5}**Cl**, and ^{3,5}**Br**. All energies are in kcal mol^{-1} relative to isolated reactants in the triplet spin state. Red and blue represent the triplet and the quintet spin mechanism, resepctively. **R** are the reactants.

Geometrically, in the quintet spin state, the substrate attacks the oxoiron group along the *z*-axis, that is, along the O−Fe−N_{axial} axis. This has been shown to occur because of favorable orbital overlap, because in the quintet spin state, an electron is transferred into the $\sigma^*_{z^2}$ orbital that is aligned along that axis.[14c,25b] In the triplet spin state, by contrast, an electron is transferred into the singly occupied π^*_{xz} orbital so that the substrate approaches the oxo group from the side. In ^{3}**TS1**(Cl,Br) structures, the substrate is far away from the oxo group, and curiously, it seems to approach in an anti-Markovnikov fashion.

As expected, the barriers in the triplet spin state are considerably higher in energy than those obtained on the quintet spin state surface, in line with previous work in the field that showed that quintet spin state oxidants are more reactive than triplet spin state ones.[18,19] In the case of chloride- and bromide-cis-substituted oxidants, the energy difference between ^{3}**TS1** and ^{5}**TS1** is more than 10 kcal mol^{-1}, whereas it is only 3.2 kcal mol^{-1} for $\mathbf{TS1}_F$. This is due to the fact that the intermediate complex $^5\mathbf{I}_F$ is less stable than $^5\mathbf{I}_{Cl}$ and $^5\mathbf{I}_{Br}$ by 18.5 and 17.4 kcal mol^{-1}, respectively, which also increases the barrier $^5\mathbf{TS1}_F$, and is the consequence of the smaller 3d-block splitting in the fluoride-substituted system, see Figure 3 above. Therefore, first-row elements interact differently with the metal than second- and third-row elements that stabilize high-spin Fe^{III} states, such as those that appear in the intermediate complexes, more in comparison to $\mathbf{I}_F$. As a consequence, the reaction barriers are lower for $^5\mathbf{TS1}_{Cl}$ and $^5\mathbf{TS1}_{Br}$. The $^3\mathbf{TS1}_F$ barrier is significantly lower than the analogous barriers for L = Cl^- and Br^- as a result of the smaller HOMO/LUMO energy gap, see Figure 3. As reasoned above, the π^*_{xy} orbitals for the systems with chloride or bromide cis ligands are significantly stabilized because a second-row element is further away from the iron atom and cannot form bonding and antibonding orbital overlap with this orbital. As a consequence, the π^*_{xy} orbital is reduced to a lone-pair (nonbonding) orbital in these systems and considerably stabilized. This results in a larger HOMO/LUMO energy gap for these systems and higher ^{3}**TS1** barriers for ^{3}**Cl** and ^{3}**Br** with respect to ^{3}**F**. On the quintet spin state surface, an electron is transferred into the $\sigma^*_{z^2}$ orbital that is located along the O−Fe−N_{axial} axis. This orbital is built up from the $3d_{z^2}$ orbital on Fe that interacts with 2p orbitals on O and N_{axial} along the same axis. The coefficients of atomic orbital contributions of the cis ligand that contribute to this molecular orbital are very small, and hence, the barriers on the quintet spin state surface show little dependence on the cis ligand.

Small differences in bond lengths are obtained between the optimized structures in Figure 5 with L = Cl^- and Br^-, and the only significant variation is found for the Fe−L bond, as expected. The systems with fluoride as cis ligand give considerable shortening of the Fe−N bond opposite to this Fe−F bond and in the triplet spin states also in the other Fe−N bonds which contrast the bond lengths observed for the systems with chloride and bromide ligands. This appears to be the result of binding of a first-row element to iron on the cis position because similar Fe−N bond distances are obtained for $^3\mathbf{I}_{NCMe}$ and $^3\mathbf{P}_{NCMe}$. Thus, when iron is bound to six first-row elements, it is located in almost the exact center of the octahedron. However, when one of those ligands is replaced by a larger element (chloride or bromide), the iron moves away from the center. This perturbation of the metal from its central position influences the molecular orbitals, charge distributions, and eventually its optimized geometries. As a result, significantly longer Fe−N distances are obtained in the chloride- and bromide-substituted systems. The interactions of the ligand with the metal are the consequence of the cis effect and cis influence and result in different molecular orbitals as shown above in Figure 2.

The molecular entropy is commonly described with partition functions for the molecular translation, rotations, and vibrations. In addition, there is also an electronic contribution that is a function of the overall spin multiplicity. Hence, high-spin states are stabilized at the free energy scale with respect to the absolute energies. In our particular systems, the free energy of activation reverses the spin-state ordering of the oxidants with L = F^- and Br^-. Thus, in the gas phase, the ΔE + ZPE values (Figure 1) imply a triplet spin ground state for all systems, but the free energy difference is reversed for the fluoride- and bromide-substituted systems. If that is the case, these systems should exist in a quintet spin ground state and react with low barriers to form epoxide products. Alternatively, the reaction will start on the triplet ground state with a triplet−quintet spin state crossing to the quintet spin state surface prior to the actual epoxidation process. The rate of the reaction is then determined by the spin state crossing.

In addition to the systems with a halide anion as cis ligand, we also tested the reaction of $[Fe^{IV}{=}O(TPA)NCCH_3]^{2+}$ with styrene. However, its reaction mechanism in the gas phase follows a completely different process from the one shown above in Figure 6. Thus, $[Fe^{IV}{=}O(TPA)NCCH_3]^{2+}$ reacts with styrene via an initial electron transfer to give styrene cation radical and $[Fe^{III}{=}O(TPA)NCCH_3]^{+}$ followed by a stepwise epoxidation mechanism of styrene cation radical via a radical intermediate. The reduction of $^3\mathbf{NCMe}^{2+}$ by styrene (S) to give $^4\mathbf{NCMe}^{+}$ is calculated to be exothermic by $\Delta G = -203.7$ kcal mol^{-1}. That should give the system sufficient energy to epoxidize styrene cation radical. Indeed, the calculations show that the complete reaction mechanism is exothermic. Therefore, $^3\mathbf{NCMe}^{2+}$ is expected to efficiently epoxidize and hydroxylate substrates because of the large energy release as a result of its reduction. The ionization potential of styrene is sufficiently low (8.46 eV)[33] to enable reduction of the iron center rather than a direct epoxidation. Moreover, $^{3,5}\mathbf{NCMe}^{2+}$ has an overall charge of +2, and the reduction of the metal by styrene will spread the charge over a much larger area. Calculations in a dielectric constant of $\varepsilon = 5.7$ lowers the exothermicity of electron transfer to −124.9 kcal mol^{-1}, but the epoxidation reaction is still overall exothermic. Therefore, $^{3,5}\mathbf{NCMe}^{2+}$ will react with styrene via an initial electron abstraction, followed by epoxidation of styrene

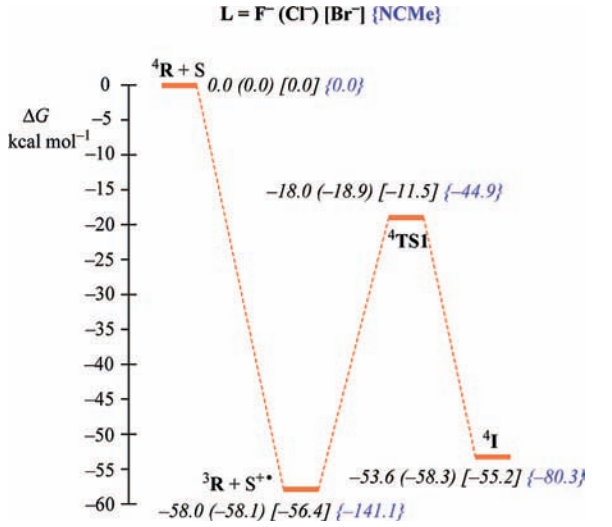

Figure 7. Free energy landscape of styrene (S) epoxidation by $^4\mathbf{F}^{2+}$, $^4\mathbf{Cl}^{2+}$, $^4\mathbf{Br}^{2+}$, and $^4\mathbf{NCMe}^{3+}$. All energies are in kcal mol^{-1} relative to isolated reactants in the quartet spin state.

cation radical with high exothermicity and high efficiency. Consequently, the apparent reactivity differences of $[Fe^{IV}{=}O(TPA)Cl]^+$ and $[Fe^{IV}{=}O(TPA)NCCH_3]^{2+}$ are the result of a different overall charge of the systems, and the actual chemical effect of the group in the cis position is small.

$$^3NCMe^{2+} + S \rightarrow {}^4NCMe^{+} + S^{+\bullet} - 203.7 \text{ kcal mol}^{-1} \quad (4)$$

Oxidizing Properties of $[Fe^{V}{=}O(TPA)L]^{(n+1)+}$. Recent experimental studies of Mas-Ballesté and Que[34] showed that apart from an $[Fe^{IV}{=}O(TPA)L]^+$ oxidant, also an $[Fe^{V}{=}O(TPA)L]^{2+}$ system may appear. Thus, in order to find out how $[Fe^{V}{=}O(TPA)L]^{2+}$ with L = F^-, Cl^-, and Br^- and $[Fe^{V}{=}O(TPA)NCCH_3]^{3+}$ react with styrene, we studied this reaction with DFT methods. The potential energy profile is shown in Figure 7, and optimized geometries of the radical intermediates are displayed in Figure 8.

Thus, similarly to the reaction of $[Fe^{IV}{=}O(TPA)NCCH_3]^{2+}$ with styrene from the previous section, also the collision of $[Fe^{V}{=}O(TPA)L]^{n+}$, L = F^-, Cl^-, Br^-, and $NCCH_3$, with styrene leads to an efficient electron transfer to form $[Fe^{IV}{=}O(TPA)L]^{(n-1)+}$ and styrene cation radical with an exothermicity of almost 60 kcal mol^{-1} for the halogen-substituted systems and −141.1 kcal mol^{-1} for $^4\mathbf{NCMe}^{3+}$. A subsequent C−O formation leads to intermediates $^4\mathbf{I}_{F,Cl,Br,NCMe}$, followed by ring closure to form epoxide products. In the case of the halogen-substituted systems, the intermediate complex ($^4\mathbf{I}_{F,Cl,Br}$) is essentially deprotonated 2-halogeno-2-phenyl-ethanol bound to an iron center. This complex is characterized by a five-membered ring of the halogen anion with the Fe, O, and C atoms, see Figure 8. As a consequence, these intermediates will form epoxides via a ring-closure barrier, C−C−O ring, with simultaneous breaking of the halogen−carbon bond of the five-membered ring. Alternatively, the deprotonated 2-halogeno-2-phenyl-ethanol can pick up a proton from the solvent to form halogenated products. However, this reaction will depend on the ability to accept protons from the solvent.

Nevertheless, the epoxidation barriers are lower in energy than the reduction of the metal center so that it may be assumed that epoxides will be the dominant products from the reaction of $[Fe^{V}{=}O(TPA)L]^{2+}$ with styrene. However, the actual oxidant

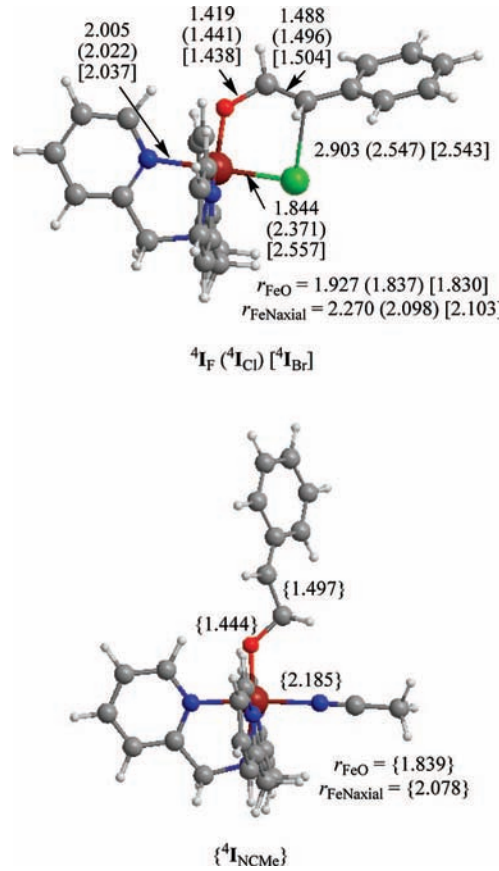

Figure 8. Optimized geometries of $^4\mathbf{I}_F$, $^4\mathbf{I}_{Cl}$, $^4\mathbf{I}_{Br}$, and $^4\mathbf{I}_{NCMe}$ with bond lengths in Angstroms.

in these reactions is the $[Fe^{IV}{=}O(TPA)L]^+$ complex that reacts with styrene cation radical.

With a neutral cis ligand such as $NCCH_3$, the interactions with the approaching substrate are missing, and no stable ring structure can be formed. As a result, the substrate approaches the iron center from the top (see the structure at the bottom of Figure 8) to reduce the electrostatic interactions with the TPA ligand. Therefore, it is not expected that the reaction of either $[Fe^{IV}{=}O(TPA)NCCH_3]^{2+}$ or $[Fe^{V}{=}O(TPA)NCCH_3]^{3+}$ will produce byproduct in which the cis ligand is incorporated, whereas oxidants with a halogen anion as cis ligand may produce these byproducts in significant amounts.

Conclusion

In summary, DFT calculations on the cis effect of oxoiron systems with a TPA tetradentate ligand have been performed. It is shown that first row elements on the cis position interact differently with the metal than second- and third-row elements. This, in turn, influences the molecular orbitals and the $t_{2g}-e_g$ orbital splitting of the metal 3d orbitals. Thus, second- and third-row elements stabilize high-spin Fe^{III} states and therefore give lower reaction barriers of epoxidation reactions. Multiply charged systems, in addition, react via an initial reduction of the metal center prior to styrene activation. This reduction creates sufficient energy to epoxidize substrates. In summary, Fe^{V} oxidants are the most efficient oxidants because of the possibility of an initial reduction of the iron center prior to the oxidizing event, which essentially acts as a cofactor.

Acknowledgment. The research was supported by CPU time provided by the National Service of Computational Chemistry

Software (NSCCS). Financial support from the Korea Science and Engineering Foundation and the Ministry of Science and Technology of Korea through the CRI Program is acknowledged.

Supporting Information Available: Cartesian coordinates of all structures described in this work, tables with group spin densities, charges and relative energies, and Figures with results of geometry scans. This material is available free of charge via the Internet at http://pubs.acs.org.

References and Notes

(1) (a) Sono, M.; Roach, M. P.; Coulter, E. D.; Dawson, J. H. *Chem. Rev.* **1996**, *96*, 2841–2888. (b) Kadish, K. M., Smith, K. M., Guilard, R. Eds. *The Porphyrin Handbook*; Academic Press: San Diego, CA, 2000. (c) Groves, J. T. *Proc. Natl. Acad. Sci. U.S.A.* **2003**, *100*, 3569–3574. (d) Ortiz de Montellano, P. R., Ed. *Cytochrome P450: Structure, Mechanism and Biochemistry*, 3rd ed.; Kluwer Academic/Plenum Publishers: New York, 2004. (e) Guengerich, F. P. *Chem. Res. Toxicol.* **2001**, *14*, 611–650.

(2) (a) Li, H.; Narasimhulu, S.; Havran, L. M.; Winkler, J. D.; Poulos, T. L. *J. Am. Chem. Soc.* **1995**, *117*, 6297–6299. (b) Schlichting, I.; Berendzen, J.; Chu, K.; Stock, A. M.; Maves, S. A.; Benson, D. E.; Sweet, R. M.; Ringe, D.; Petsko, G. A.; Sligar, S. G. *Science* **2000**, *287*, 1615–1622. (c) Veitch, N. C.; Smith, A. T. *Adv. Inorg. Chem.* **2000**, *51*, 107–162.

(3) (a) Dawson, J. H.; Holm, R. H.; Trudell, J. R.; Barth, G.; Linder, R. E.; Bunnenberg, E.; Djerassi, C.; Tang, S. C. *J. Am. Chem. Soc.* **1976**, *98*, 3707–3709. (b) Poulos, T. L. *J. Biol. Inorg. Chem.* **1996**, *1*, 356–359.

(4) Gross, Z.; Nimri, S. *Inorg. Chem.* **1994**, *33*, 1731–1732.

(5) (a) Czarnecki, K.; Nimri, S.; Gross, Z.; Proniewicz, L. M.; Kincaid, J. R. *J. Am. Chem. Soc.* **1996**, *118*, 2929–2935. (b) Sastri, C. V.; Park, M. J.; Ohta, T.; Jackson, T. A.; Stubna, A.; Seo, M. S.; Lee, J.; Kim, J.; Kitagawa, T.; Münck, E.; Que, L., Jr.; Nam, W. *J. Am. Chem. Soc.* **2005**, *127*, 12494–12495.

(6) Gross, Z. *J. Biol. Inorg. Chem.* **1996**, *1*, 368–371.

(7) (a) Nam, W.; Lim, M. H.; Oh, S.-Y.; Lee, J. H.; Lee, H. J.; Woo, S. K.; Kim, C.; Shin, W. *Angew. Chem., Int. Ed.* **2000**, *39*, 3646–3649. (b) Rohde, J.-U.; Que, L., Jr. *Angew. Chem., Int. Ed.* **2005**, *44*, 2255–2258.

(8) Kamachi, T.; Kouno, T.; Nam, W.; Yoshizawa, K. *J. Inorg. Biochem.* **2006**, *100*, 751–754.

(9) Groves, J. T.; Gross, Z.; Stern, M. K. *Inorg. Chem.* **1994**, *33*, 5065–5072.

(10) (a) Song, W. J.; Ryu, Y. O.; Song, R.; Nam, W. *J. Biol. Inorg. Chem.* **2005**, *10*, 294–304. (b) Nam, W. *Acc. Chem. Res.* **2007**, *40*, 522–531.

(11) (a) de Visser, S. P.; Ogliaro, F.; Sharma, P. K.; Shaik, S. *Angew. Chem., Int. Ed* **2002**, *41*, 1947–1951. (b) de Visser, S. P.; Ogliaro, F.; Sharma, P. K.; Shaik, S. *J. Am. Chem. Soc.* **2002**, *124*, 11809–11826.

(12) (a) Takahashi, A.; Kurahashi, T.; Fujii, H. *Inorg. Chem.* **2007**, *46*, 6227–6229. (b) de Visser, S. P. *J. Phys. Chem. B* **2007**, *111*, 12299–12302.

(13) (a) Sastri, C. V.; Lee, J.; Oh, K.; Lee, Y. J.; Lee, J.; Jackson, T. A.; Ray, K.; Hirao, H.; Shin, W.; Halfen, J. A.; Kim, J.; Que, L., Jr.; Shaik, S.; Nam, W. *Proc. Natl. Acad. Sci. U.S.A.* **2007**, *104*, 19181–19186. (b) Hirao, H.; Que, L., Jr.; Nam, W.; Shaik, S. *Chem. Eur. J.* **2008**, *14*, 1740–1756.

(14) (a) Shaik, S.; de Visser, S. P.; Ogliaro, F.; Schwarz, H.; Schröder, D. *Curr. Opin. Chem. Biol.* **2002**, *6*, 556–567. (b) Shaik, S.; Kumar, D.; de Visser, S. P.; Altun, A.; Thiel, W. *Chem. Rev.* **2005**, *105*, 2279–2328. (c) Hirao, H.; Kumar, D.; Que, L., Jr.; Shaik, S. *J. Am. Chem. Soc.* **2006**, *128*, 8590–8606.

(15) Zhou, Y.; Shan, X.; Mas-Ballesté, R.; Bukowski, M. R.; Stubna, A.; Chakrabarti, M.; Slominski, L.; Halfen, J. A.; Münck, E.; Que Jr., L. *Angew. Chem., Int. Ed.* **2008**, *47*, 1896–1899.

(16) Rohde, J.-U.; Stubna, A.; Bominaar, E.; Münck, E.; Nam, W.; Que, L., Jr *Inorg. Chem.* **2006**, *45*, 6435–6445.

(17) Noack, H.; Siegbahn, P. E. M. *J. Biol. Inorg. Chem.* **2007**, *12*, 1151–1162.

(18) (a) de Visser, S. P. *J. Am. Chem. Soc.* **2006**, *128*, 9813–9824. (b) Aluri, S.; de Visser, S. P. *J. Am. Chem. Soc.* **2007**, *129*, 14846–14847.

(19) de Visser, S. P.; Oh, K.; Han, A.-R.; Nam, W. *Inorg. Chem.* **2007**, *46*, 4632–4641.

(20) *Jaguar 7.0*; Schrödinger L. L. C.: Portland, OR, 2007.

(21) Frisch, M. J.; Trucks, G. W.; Schlegel, H. B.; Scuseria, G. E.; Robb, M. A.; Cheeseman, J. R.; Montgomery, J. A., Jr.; Vreven, T.; Kudin, K. N.; Burant, J. C.; Millam, J. M.; Iyengar, S. S.; Tomasi, J.; Barone, V.; Mennucci, B.; Cossi, M.; Scalmani, G.; Rega, N.; Petersson, G. A.; Nakatsuji, H.; Hada, M.; Ehara, M.; Toyota, K.; Fukuda, R.; Hasegawa, J.; Ishida, M.; Nakajima, T.; Honda, Y.; Kitao, O.; Nakai, H.; Klene, M.; Li, X.; Knox, J. E.; Hratchian, H. P.; Cross, J. B.; Bakken, V.; Adamo, C.; Jaramillo, J.; Gomperts, R.; Stratmann, R. E.; Yazyev, O.; Austin, A. J.; Cammi, R.; Pomelli, C.; Ochterski, J. W.; Ayala, P. Y.; Morokuma, K.; Voth, G. A.; Salvador, P.; Dannenberg, J. J.; Zakrzewski, V. G.; Dapprich, S.; Daniels, A. D.; Strain, M. C.; Farkas, O.; Malick, D. K.; Rabuck, A. D.; Raghavachari, K.; Foresman, J. B.; Ortiz, J. V.; Cui, Q.; Baboul, A. G.; Clifford, S.; Cioslowski, J.; Stefanov, B. B.; Liu, G.; Liashenko, A.; Piskorz, P.; Komaromi, I.; Martin, R. L.; Fox, D. J.; Keith, T.; Al-Laham, M. A.; Peng, C. Y.; Nanayakkara, A.; Challacombe, M.; Gill, P. M. W.; Johnson, B.; Chen, W.; Wong, M. W.; Gonzalez, C.; Pople, J. A. *Gaussian 03*, revision C.02; Gaussian, Inc.: Wallingford, CT, 2004.

(22) (a) Becke, A. D. *J. Chem. Phys.* **1993**, *98*, 5648–5652. (b) Lee, C.; Yang, W.; Parr, R. G. *Phys. Rev. B* **1988**, *37*, 785–789.

(23) Hay, P. J.; Wadt, W. R. *J. Chem. Phys.* **1985**, *82*, 270–283.

(24) Scott, A. P.; Radom, L. *J. Phys. Chem.* **1996**, *100*, 16502–16513.

(25) (a) Green, M. T. *J. Am. Chem. Soc.* **1999**, *121*, 7934–7940. (b) de Visser, S. P. *J. Am. Chem. Soc.* **2006**, *128*, 15809–15818.

(26) de Visser, S. P. *J. Phys. Chem. A* **2005**, *109*, 11050–11057.

(27) For experimental data on oxoiron complexes, see, for example, (a) Riggs-Gelasco, P. J.; Price, J. C.; Guyer, R. B.; Brehm, J. H.; Barr, E. W.; Bollinger Jr., J. M.; Krebs, C. *J. Am. Chem. Soc.* **2004**, *126*, 8108–8109. (b) Bukowski, M. R.; Koehntop, K. D.; Stubna, A.; Bominaar, E. L.; Halfen, J. A.; Münck, E.; Nam, W.; Que, L., Jr. *Science* **2005**, *310*, 1000–1002. (c) de Oliveira, F. T.; Chanda, A.; Banerjee, D.; Shan, X.; Mondal, S.; Que, L., Jr.; Bominaar, E. L.; Münck, E.; Collins, T. J. *Science* **2007**, *315*, 835–838.

(28) (a) Ogliaro, F.; de Visser, S. P.; Groves, J. T.; Shaik, S. *Angew. Chem., Int. Ed.* **2001**, *40*, 2874–2878. (b) Ogliaro, F.; de Visser, S. P.; Cohen, S.; Kaneti, J.; Shaik, S. *ChemBioChem* **2001**, *2*, 848–851. (c) de Visser, S. P.; Shaik, S.; Sharma, P. K.; Kumar, D.; Thiel, W. *J. Am. Chem. Soc.* **2003**, *125*, 15779–15788.

(29) Green, M. T. *J. Am. Chem. Soc.* **2006**, *128*, 1902–1906.

(30) (a) Badger, R. M. *J. Chem. Phys.* **1934**, *2*, 128–131. (b) Herschbach, D. R.; Laurie, V. W. *J. Chem. Phys.* **1961**, *35*, 458–464.

(31) (a) Ogliaro, F.; de Visser, S. P.; Shaik, S. *J. Inorg. Biochem.* **2002**, *91*, 554–567. (b) Wang, R.; de Visser, S. P. *J. Inorg. Biochem.* **2007**, *101*, 1464–1472.

(32) (a) de Visser, S. P.; Ogliaro, F.; Harris, N.; Shaik, S. *J. Am. Chem. Soc.* **2001**, *123*, 3037–3047. (b) de Visser, S. P.; Ogliaro, F.; Shaik, S. *Angew. Chem., Int. Ed.* **2001**, *40*, 2871–2874. (c) Kumar, D.; de Visser, S. P.; Shaik, S. *Chem. Eur. J.* **2005**, *11*, 2825–2835.

(33) (a) Lias, S. G. In *Ionization Energy Evaluation in NIST Chemistry WebBook, NIST Standard Reference Database Number 69*; Linstrom, P. J., Mallard, W. G. Eds.; National Institute of Standards and Technology: Gaithersburg MD, June 2005; 20899 (http://webbook.nist.gov). (b) Dyke, J. M.; Ozeki, H.; Takahashi, M.; Cockett, M. C. R.; Kimura, K. *J. Chem. Phys.* **1992**, *97*, 8926–8933.

(34) Mas-Ballesté, R.; Que Jr, L. *J. Am. Chem. Soc.* **2007**, *129*, 15964–15972.

JP8018556